Theory, validation and application of blind source separation to diffusion MRI for tissue characterisation and partial volume correction

Miguel Molina-Romero[1,2], Pedro A Gómez[1,2], Jonathan I Sperl[2], Andrew J Stewart[3], Derek K Jones[4], Marion I Menzel[2], Bjoern H Menze[1]

[1]Computer Science, Technische Universität München, Munich, Germany
[2]GE Global Research, Munich, Germany
[3]EMRIC, Cardiff University, Cardiff, UK
[4]CUBRIC School of Psychology, Cardiff University, Cardiff, UK

Abstract. Here we present blind source separation (BSS) as a new tool to analyse multi-echo diffusion data. This technique is designed to separate mixed signals and is widely used in audio and image processing. Interestingly, when it is applied to diffusion MRI, we obtain the diffusion signal from each water compartment, what makes BSS optimal for partial volume effects correction. Besides, tissue characteristic parameters are also estimated. Here, we first state the theoretical framework; second, we optimise the acquisition protocol; third, we validate the method with a two compartments phantom; and finally, show an in-vivo application of partial volume correction.

1 Purpose

The compartmental nature of tissue is generally accepted [1,7,11,14,17,19]. The diffusion-weighted MRI (dMRI) signal depends on the relaxation times of the compartments ($T2_i$), their diffusivities (D_i), volume fractions (f_i) and proton density (S_0). The simultaneous contribution of these parameters results in a lack of specificity to each independent effect and induces a bias [13,16] on the diffusion metrics known as partial volume contamination. Specificity and partial volume correction problems have been addressed independently [2,6,9,13,14]. Here we present blind source separation (BSS) as a new approach in dMRI that separates mixed signals and yields tissue microstructure parameters, tackling both problems at once.

2 Methods

2.1 Theory

This method is based on three assumptions: 1) tissue is made of water compartments with different diffusivities [6,14]; 2) there is no water exchange [1]; and 3) each compartment has a different $T2$ [6,11,14]. Hence, we can describe the

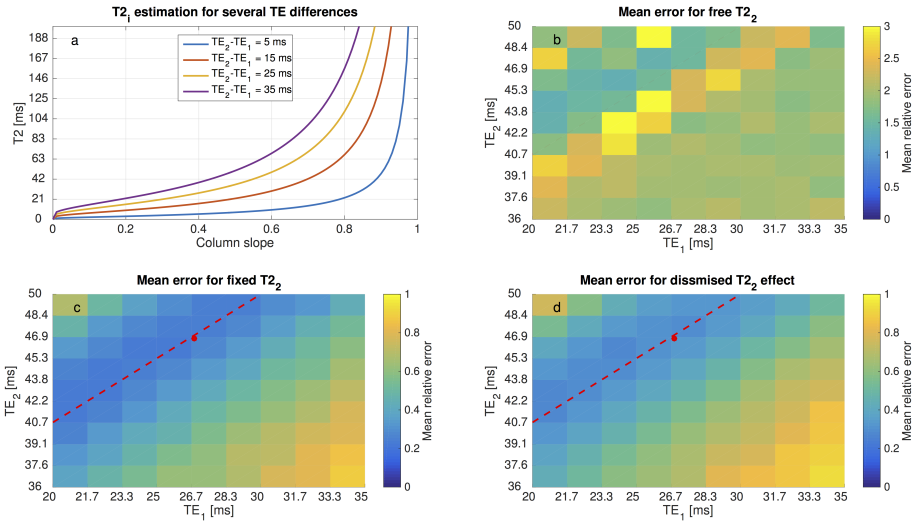

Fig. 1. (b-d) Mean error of the parameter estimations. (a) Relationship between the slope of the columns of $\mathbf{A}$ and the estimation of $T2$ for several TE differences. When the slope of the columns tends towards 1 ($T2 \gg TE$), the estimation of $T2$ is in the asymptotic region and thus uncertain. This uncertainty can be observed in (b) where the minimum error is larger than in (c,d) for fixed $T2_2$ and dismissed $T2_2$ effect. Notice that the optimal TE pairs are marked by the red dashed lines. The red dots mark the TE pair used for phantom validation experiment.

measured diffusion signal as the weighted sum of the compartmental sources. These weights depend only on the volume fraction (f) and the ratio between the compartmental $T2_i$ and the experimental TE_j. Therefore, varying TE modifies the weights and the system can be expressed as a BSS problem:

$$\begin{bmatrix} X(TE_1, \Delta, q) \\ \vdots \\ X(TE_M, \Delta, q) \end{bmatrix} = \begin{bmatrix} f_1 e^{TE_1/T2_1} & \cdots & f_N e^{TE_1/T2_N} \\ \vdots & \ddots & \vdots \\ f_1 e^{TE_M/T2_1} & \cdots & f_N e^{TE_M/T2_N} \end{bmatrix} \begin{bmatrix} S_1(\Delta, q) \\ \vdots \\ S_N(\Delta, q) \end{bmatrix} S_0 \qquad (1)$$

$$\mathbf{X} = \mathbf{AS}, \qquad (2)$$

where $\mathbf{X}$ are the measurements for several TEs, $\mathbf{A}$ the mixing matrix, $\mathbf{S}$ the compartmental diffusion source, M the number of measurements, and N the number of compartments. Here, among the possible BSS solutions [18], and unlike in [12], we use a sparsifying transform [15] followed by non-negative sparse coding [8].

Here we focus on two-compartment environments ($N = M = 2$). Besides, when $T2_i$ is larger than the TEs (i.e. CSF), the exponential term can be dismissed ($\exp(TE_j/T2_i) \approx 1$) and thus the $T2_i$. Alternatively, $T2_i$ can be fixed to

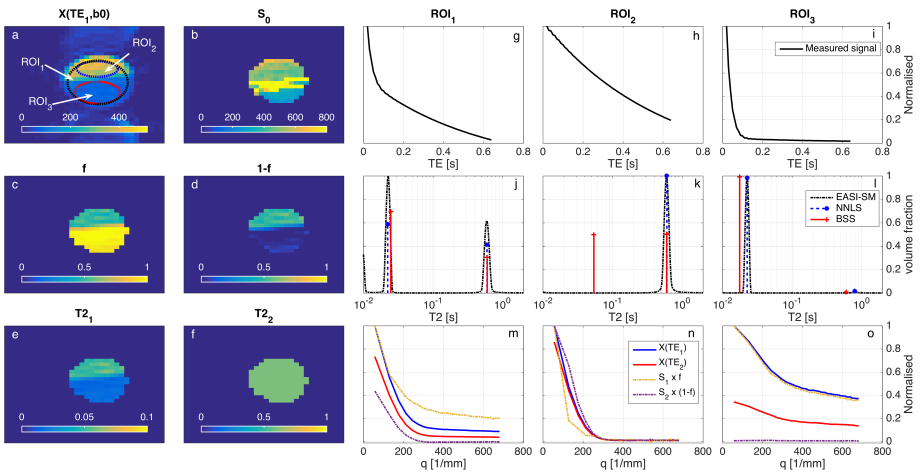

Fig. 2. (a) b0 image at $TE_1 = 26\ ms$ with ROIs overlaid. Each ROI represents a possible case: ROI_1 ($f \approx 0.5$), whole phantom; ROI_2 ($f \approx 0$), water; ROI_3 ($f \approx 1$), yeast. (b) Signal intensity at $TE = 0\ ms$. Volume fractions for the associated intra-cellular (c) and extra-cellular (d) compartments. $T2$ for the intra-cellular (e) and extra-celullar (f) cell compartments. Averaged multi-echo signal for each ROI (g,h,i) and the corresponding $T2$ spectral fitting with NNLS and EASI-SM (j,k,l) compared with the volume fractions and $T2$s estimated by BSS ($T2_2$ fixed at 0.6 s according to NNLS and EASI-SM). Measured and separated diffusion signals for each ROI (m,n.o).

an expected value if prior knowledge is available (i.e. $\text{T2}_{CSF} \approx 2\ s$ 6). We study the effect both approximations on the error of the parameter estimation.

We perform three experiments to: 1) find the range of optimal TEs; 2) validate our method; and 3) show an application. Figure 4 contains the experimental details.

2.2 Optimisation simulations

Tissue with two compartments was simulated with known $T2$s (22 and 597 ms) for restricted and free diffusion signals [4]. We ran a simulation experiment varying TE and f (11 points) to calculate the mean error for all the parameter combinations and find the optimal TE region for free, fixed and dismissed $T2_2$.

2.3 Phantom validation

For validation, we used a phantom made of yeast and water (1:1) as a two compartments sample [5]. A multi-echo experiment was acquired and $T2$s fitted with NNLS [10] and EASI-SM [3]. Besides, BSS was applied on the diffusion dataset fixing $T2_2 = 0.6\ s$ (NNLS). Finally, results from the three methods were compared.

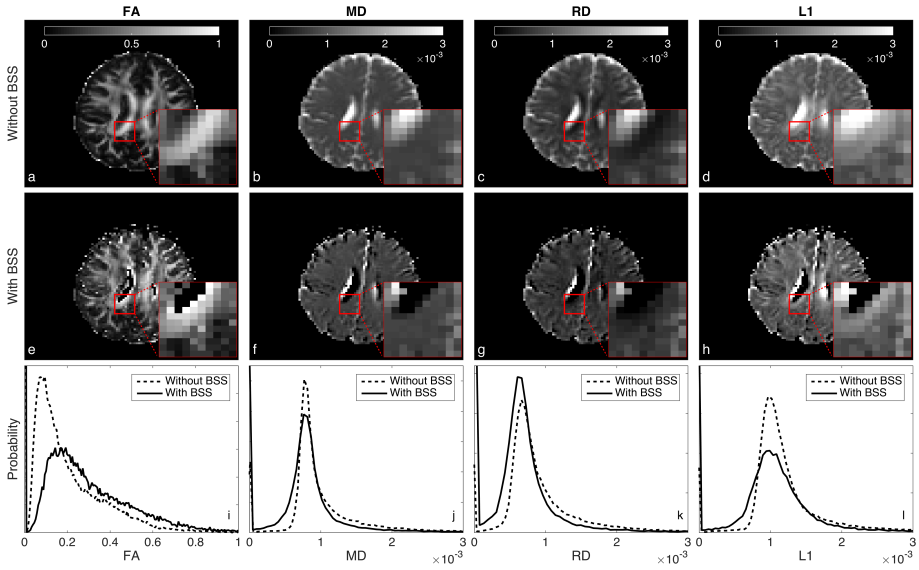

Fig. 3. Comparison of DTI metrics with and without CSF contamination correction by BSS. Histograms of values for the whole brain (i-l) show an increase of FA, and a decrease of MD, RD and L1. Both effects are consistent with the elimination of the CSF contribution. Besides, we observe a significant increase of FA in the borders of the ventricles (zoomed area), where the contamination is expected to be high. Notice that BSS mostly crops the ventricles and the external CSF and increases the contrast of the white matter.

2.4 In vivo

A young female volunteer went under a DTI acquisition. CSF signal was extracted from the data using BSS, fixing $T2_2 = 2\ s$ [11]. Finally, DTI metrics with and without correction were compared.

3 Results and discussion

3.1 Optimisation simulations

Fig 1a depicts $T2$ versus the slope of a column of $\mathbf{A}$. As the slope tends towards 1, the estimation falls into an asymptotic region increasing the uncertainty on the $T2$ estimation. Therefore, fixing its value or dismissing its contribution reduces the mean error of the parameter estimations (Fig. 1b-d). Moreover, fixing the $T2$ value performs slightly better than dismissing its effect (Fig. 1c-d).

3.2 Phantom validation

Fig.2g-o compare the results of BSS against NNLS and EASI-SM in a ROI-based analysis. Fig. 2j,l show agreement of $T2_1$ and f with NNLS and EASI-SM for

		Optimisation	Validation	In-Vivo
Diffusion acquisition	TR	Inf	3 s	4 s
	TE_1	20-35 ms (10 points)	26 ms	73 ms
	TE_2	36-50 ms (10 points)	46 ms	110 ms
	#Diffusion directions	1	1	41
	#b-values	33	33	2
	Range of b-values	0-13504 s/mm^2	70-10048 s/mm^2	0-1000 s/mm^2
	Reverse polarity	No	No	Yes
	Resolution	1 voxel	32x32	96x96
	Sequence	PGSE	STEAM	PGSE
T2 mapping	TR		2.5 s	
	#TEs		64	
	Range of TEs		10-640 ms	
	NEX		4	
	Resolution		32x32	
	Sequence		SE	
	Scanner	Simulated	9.4T Biospec 94/20 (Bruker, Ettlingen, Germany)	3T HDx MRI (GE, Milwaukee, WI)

Fig. 4. Experimental setups for the optimisation simulation, the phantom validation and the in-vivo experiment.

ROI_1 and ROI_3. Besides, in Fig. 1m, S_1 (associated with intra-cellular space) describes a restricted diffusion signal similar as in Fig 2o, and S_2 (associated with extra-cellular space) shows a free diffusion behaviour as in Fig. 2n. Both findings are in agreement with the simulations and indicate that BSS successfully separates signals from two compartments. Interestingly, BSS disentangles measurements from ROI_2 into two similar and equally scaled sources (Fig. 2n) indicating that only one source exists. For illustration, Fig. 2b-f show that the voxel-based maps generated with BSS are consistent with the ROI based analysis.

3.3 In vivo

In Fig. 3, with BSS, we observe an increase of the fractional anisotropy (FA) (a,e,i) and a reduction of the mean diffusivity (MD) (b,f,j), radial diffusivity (RD) (c,g,k), and tensor's main eigenvalue (L1) (d,h,l). This is consistent with the elimination of the CSF contribution. Also, we notice that with BSS the ventricles are extracted and white matter structures are better defined, especially the voxels at the border of the ventricles (zoomed area).

4 Conclusions

Here we show that BSS of diffusion data is a suitable technique to separate compartmental sources. We demonstrate that this method is appropriate for partial volume correction. Besides, tissue volume fraction, relaxation and diffusivity parameters are estimated allowing for simultaneous tissue characterisation.

5 Acknowledgments

With the support of the TUM Institute for Advanced Study, funded by the German Excellence Initiative and the European Commission under Grant Agreement Number 605162.

References

1. Assaf, Y., Basser, P.J.: Composite hindered and restricted model of diffusion (CHARMED) MR imaging of the human brain. NeuroImage 27, 48–58 (2005)
2. Benjamini, D., Basser, P.J.: Use of marginal distributions constrained optimization (MADCO) for accelerated 2D MRI relaxometry and diffusometry. Journal of Magnetic Resonance 271, 40–45 (2016)
3. Björk, M., Zachariah, D., Kullberg, J., Stoica, P.: A multicomponent T 2 relaxometry algorithm for myelin water imaging of the brain. Magnetic Resonance in Medicine (2015)
4. Cook, P.A., Bai, Y., Nedjati-Gilani, S., Seunarine, K.K., Hall, M.G., Parker, G.J., Alexander, D.C.: Camino: Open-Source Diffusion-MRI Reconstruction and Processing. Proc Intl Soc Mag Reson Med (2014)
5. Cory, D.G.: Measurement of translational displacement probabilities by NMR: An indicator of compartmentation. Magnetic Resonance in Medicine 14(3), 435–444 (1990)
6. Does, M.D., Gore, J.C.: Compartmental study of diffusion and relaxation measured in vivo in normal and ischemic rat brain and trigeminal nerve. Magnetic resonance in medicine 43(6), 837–44 (2000)
7. Ferizi, U., Schneider, T., Witzel, T., Wald, L.L., Zhang, H., Wheeler-Kingshott, C.A., Alexander, D.C.: White matter compartment models for in vivo diffusion MRI at 300mT/m. NeuroImage 118, 468–483 (2015)
8. Hoyer, P.: Non-negative sparse coding. In: Proceedings of the 12th IEEE Workshop on Neural Networks for Signal Processing. pp. 557–565. IEEE (2002)
9. Kim, D., Kim, J.H., Haldar, J.P.: Diffusion-Relaxation Correlation Spectroscopic Imaging (DR-CSI): An Enhanced Approach to Imaging Microstructure. Proc Intl Soc Mag Reson Med (2016)
10. Lawson, C.L., Hanson, R.J.: Solving Least Squares Problems. Society for Industrial and Applied Mathematics (1995)
11. Mackay, A., Laule, C., Vavasour, I., Bjarnason, T., Kolind, S., M7dler, B.: Insights into brain microstructure from the T 2 distribution. Magnetic Resonance Imaging 24, 515–525 (2006)
12. Molina-Romero, M., Gómez, P.A., Sperl, J.I., Jones, D.K., Menzel, M.I., Menze, B.H.: Tissue microstructure characterisation through relaxometry and diffusion MRI using sparse component analysis. ISMRM Workshop on Breaking the Barriers of Diffusion MRI (2016)

13. Pasternak, O., Sochen, N., Gur, Y., Intrator, N., Assaf, Y.: Free water elimination and mapping from diffusion MRI. Magnetic Resonance in Medicine 62(3), 717–730 (2009)
14. Peled, S., Cory, D.G., Raymond, S.A., Kirschner, D.A., Jolesz, F.A.: Water diffusion, T(2), and compartmentation in frog sciatic nerve. Magnetic resonance in medicine 42(5), 911–8 (1999)
15. Ravishankar, S., Bresler, Y.: 0 Sparsifying Transform Learning with Efficient Optimal Updates and Convergence Guarantees. arXiv preprint arXiv:11501.02859 pp. 1–16 (2015)
16. Santis, S.D., Assaf, Y., Jones, D.: The influence of T2 relaxation in measuring the restricted volume fraction in diffusion MRI. Proc Intl Soc Mag Reson Med (2016)
17. Stanisz, G.J., Wright, G.A., Henkelman, R.M., Szafer, A.: An analytical model of restricted diffusion in bovine optic nerve. Magnetic Resonance in Medicine 37(1), 103–111 (1997)
18. Yu, X., Hu, D., Xu, J.: Blind source separation: theory and applications. Wiley (2014)
19. Zhang, H., Schneider, T., Wheeler-Kingshott, C.A., Alexander, D.C.: NODDI: Practical in vivo neurite orientation dispersion and density imaging of the human brain. NeuroImage 61(4), 1000–1016 (2012)